Sharp-Interface Formation during Lithium Intercalation into Silicon

Esteban Meca* Andreas Münch† Barbara Wagner*‡

February 25, 2016

Abstract

In this study we present a phase-field model that describes the process of intercalation of Li ions into a layer of an amorphous solid such as a-Si. The governing equations couple a viscous Cahn-Hilliard-Reaction model with elasticity in the framework of the Cahn-Larché system. We discuss the parameter settings and flux conditions at the free boundary that lead to the formation of phase boundaries having a sharp gradient in ion concentration between the initial state of the solid layer and the intercalated region. We carry out a matched asymptotic analysis to derive the corresponding sharp-interface model that also takes into account the dynamics of triple points where the sharp interface in the bulk of the layer intersects the free boundary. We numerically compare the interface motion predicted by the sharp-interface model with the long-time dynamics of the phase-field model.

Key words. Asymptotic Analysis, Phase-Field Model, Interface Dynamics, Numerical Methods

AMS subject classification 74N20, 35Q74, 35B25, 74S10

1 Introduction

Silicon electrodes for lithium-ion batteries are currently the subject of very intense research to make silicon a practical alternative to graphite. Silicon can store a large amount of lithium, but the large stresses that these electrodes undergo tend to cause their fracture and pulverization after a few cycles. Various investigations to circumvent these problems have led to designs of nanostructured electrodes such as arrays of pillars or nanowires.

However, in order to carry out systematic and knowledge-based optimizations a fundamental understanding of the mechanisms involved in the intercalation process of silicon

*Weierstrass Institute, Mohrenstraße 39, 10117 Berlin, Germany

†Mathematical Institute, University of Oxford, Andrew Wiles Building, Woodstock Road, Oxford, OX2 6GG

‡Technische Universität Berlin, Institute of Mathematics, Straße des 17. Juni 136, 10623 Berlin, Germany

itself is needed. This has lead to a number of experimental and theoretical investigations, partly with, seemingly, contradictory results. In particular, the experiments of Sethuraman et al. [28] on the stress evolution of a silicon electrode during intercalation have had a great impact on the modeling of silicon electrodes, as they have been taken as a proof of the surprising result that lithiated amorphous silicon behaves plastically, see for example the analysis in Bower et al. [2]. Their analysis is based on the assumption that the film of amorphous silicon is thin enough with respect to the substrate to which it is attached, so that the stress can be assumed uniform in the whole amorphous silicon film. However, while the thickness of the film can be controlled, the uniformity of the stress is an unknown In fact, it has been shown recently in Huang et al. [14] and Ngo et al.[24]that this assumption uniformity of stress can indeed obscure the interpretation of the results.

In addition, as has been shown more recently in Levitas et al. [18], the theoretical yield stress is never reached which has lead to some phenomenological modeling to explain yielding [33], sometimes also discarding plasticity [18]. On the other hand, the models used to take into account plasticity have problems in the determination of the parameters, sometimes suggesting a power law with exponent as high as 50 for the constitutive law [4], which can be taken as a hint that the model may not be complete. Further analysis for different electrode geometries involving cylindrical and spherical silicon particles as well as annular structures have been carried out to investigate stress evolution and deformation of lithiated silicon, see [9, 6, 7].

On the other hand, regarding the stuctural properties of silicon, it is known that after the first intercalation cycle, the original crystalline silicon becomes amorphous, see the review by McDowell et al. [21] and references therein. Moreover, as it has been shown in McDowell et al.[20] and Wang et al.[30], the first intercalation of crystalline as well as amorphous silicon occurs through a two-phase mechanism. The question whether this two-phase process also occurs in amorphous silicon in subsequent intercalation cycles has been raised in [20, 19] and a recent study by Cubuk et al. [8] based on molecular dynamics simultations relates the two-phase lithiation of amorphous silicon with a sharp structural transition in amorphous Li_xSi for $x \approx 2$ between a phase in which the Li atoms are embedded in a covalent silicon matrix to a phase in which Si atoms are packed in small clusters with few covalent bonds between them, surrounded by a dense, amorphous structure of Li atoms, suggesting a transition from a mechanically Si-like phase to a softer Li-like phase. Moreover, experiments show that this two-phase lithiation is self-limiting in nanowires [19], presumedbly due to the high stresses generated.

In Meca et al. [22] a phase-field model that couples a viscous Cahn-Hilliard-Reaction model with elasticity has been derived to describe the process of intercalation of Li-ions into a layer of an amorphous silicon and investigate conditions leading in the long-time limit to the formation of sharp phase boundaries between the original silicon phase and the lithiated phase. The analysis of the long time dynamics of the emerging sharp phase boundaries is the subject of the present study.

After presenting the phase-field formulation in Section 2, we show in the remainder of this paper how an intercalation process is nucleated, for example due to some defect

on the free absorbing boundary of a layer (or nanowire), and upon reaching a critical lithium concentration, a phase transition sets in, which in turn leads to a sharp phase boundary that then moves into the bulk of the layer and along its free boundary.

In Section 3 we derive for this regime a sharp-interface model using matched asymptotic expansions, whereby the analysis is divided into three regions, the sharp interface analysis in the bulk of the layer, the analysis close to the free boundary and the analysis of the triple points, where the sharp interface in the bulk of the layer intersects the free boundary. All three regions have to be matched and finally yield the sharp-interface model. Finally, we investigate in Section 4 numerically the dynamics of the long-time limit of the phase-field model and compare evolution of the emerging phase boundaries with expression for the velocities found from matched asymptotic analysis.

2 Formulation of the phase-field model

The system we consider consists of a thin layer of amorphous silicon resting on an undeformable substrate. Lithium enters in the layer as a consequence of the difference of electrochemical potential with the electrolyte. As the lithium concentration is increased, the layer experiences a phase transformation from a poorly lithiated phase (a-Si) to a heavily lithiated one (Li_xSi with x> 2). Lithium insertion causes a stress-free strain. For a discussion of the role of phase transformation on stress for this process we have formulated a mathematical model in Meca et al. [22] and we will briefly introduce the complete phase-field model here.

To facilitate the discussion of the results we confine our description of elasticity to linear elasticity and follow the standard approach to the coupling of phase transitions with linear elasticity, see e.g. [10] for details. From Hooke's law the elastic energy is given by

$$W = \frac{1}{2} C_{ijkl} \left(\epsilon_{ij} - \epsilon^0_{ij}\right) \left(\epsilon_{kl} - \epsilon^0_{kl}\right) \tag{2.1}$$

where the fourth order tensor C_{ijkl} is defined as the *elasticity tensor* or as the *stiffness tensor*, ϵ_{ij} denotes the *strain tensor*

$$\epsilon_{ij} = \frac{1}{2} \left(\partial_j u_i + \partial_i u_j\right) \tag{2.2}$$

defined by the *displacement field* $\mathbf{u}$, as the difference between the actual position of a material point and the position in the undeformed material $\mathbf{x}$ (reference configuration). The *stress-free strain tensor*, that is, the strain due e.g. to composition changes in the absence of stress, is assumed to grow linearly with the concentration:

$$\epsilon^0_{ij} = \alpha \left(c - \bar{c}\right) \delta_{ij} \tag{2.3}$$

where α and $\bar{c}$ are constants, possibly depending on the phase. Note that this choice implies an isotropic strain change with concentration, but this needs not to be the case and more general relations are possible.

Using the symmetries of C_{ijkl} the choice of elastic energy implies for the *stress tensor*

$$\sigma_{ij} = C_{ijkl}\left(\epsilon_{kl} - \epsilon^0_{kl}\right), \tag{2.4}$$

and assuming that the timescale of the elastic relaxation is much faster than that of diffusion or the phase transformation, elastic equilibrium implies that the divergence of the stress tensor is zero:

$$\partial_j \sigma_{ij} = 0. \tag{2.5}$$

Equation (2.5) will have to be fulfilled separately at each phase in the layer and it can be written explicitly in terms of the displacement field using

$$\sigma_{ij} = \frac{E}{1+\nu}\left(\epsilon^M_{ij} + \frac{\nu}{1-2\nu}\epsilon^M_{kk}\delta_{ij}\right), \tag{2.6}$$

where E is *Young's modulus*, ν is *Poisson's ratio* and $\epsilon^M_{ij} = \epsilon_{ij} - \epsilon^0_{ij}$ is the *mechanical strain*, the difference between the strain tensor and the stress-free strain tensor.

For the present problem the elastic properties of both phases are assumed different. We limit this difference to Young's modulus, since according to Shenoy et al. [29] there is no clear tendency in the variation of ν and obtain the equation:

$$\begin{aligned}\frac{1}{2}\frac{E'}{E}\nabla c\left(\nabla\mathbf{u} + \nabla\mathbf{u}^T\right) - \frac{E'}{E}\frac{1+\nu}{1-2\nu}\alpha(c-\bar{c})\nabla c + \frac{E'}{E}\frac{\nu}{1-2\nu}\left(\nabla\cdot\mathbf{u}\right)\nabla c \\ + \frac{1}{2}\nabla^2\mathbf{u} + \frac{1}{2(1-2\nu)}\nabla\left(\nabla\cdot\mathbf{u}\right) - \alpha\frac{1+\nu}{1-2\nu}\nabla c = 0\end{aligned} \tag{2.7}$$

where E' is the derivative of Young's modulus with respect to concentration c.

For the transport of concentration c we use the viscous Cahn-Hilliard model

$$\partial_t c = \nabla\cdot\left(M(c)\nabla\left(\mu + \chi\,\varepsilon\,\partial_t c\right)\right), \tag{2.8}$$

where $M(c)$ is the *mobility function*, which, in the present study, is taken to be a constant. The last term is the *viscous term*, see [25] and χ corresponds to a parameter with dimensions of viscosity. The chemical potential

$$\mu = \frac{1}{N_\Omega}\frac{\delta\mathcal{F}}{\delta c} = -\gamma\varepsilon\,\nabla^2 c + \frac{\gamma}{\varepsilon}\frac{1}{2}c(1-c)(1-2c) + \partial_c W(\epsilon_{ij}, c), \tag{2.9}$$

is the variational derivative of the free energy

$$\mathcal{F} = N_\Omega\int_\Omega \frac{1}{2}\gamma\varepsilon\,|\nabla c|^2 + \frac{\gamma}{\varepsilon}f(c) + W(\epsilon_{ij}, c) \tag{2.10}$$

where $f(c)$ is the usual double-well potential (free energy per particle) and $W(\epsilon_{ij}, c)$ is the elastic energy as defined in Eq. (2.1) for an isotropic elasticity tensor. The constant γ carries the dimensions of energy times length, and N_Ω is the (global) number of particles per surface. The parameter ε is related with the interface width and the interfacial energy between the lithiated and the unlithiated phases.

We nondimensionalize eqs. (2.7) and (2.8) via

$$\mu = \mu^* \gamma H_0^{-1}, \quad x = x^* H_0, \quad y = y^* H_0, \quad t = t^* H_0^3 M^{-1} \gamma^{-1}, \quad \varepsilon = \varepsilon^* H_0,$$

denoting with * the nondimensionalized variables. The characteristic length scale H_0 corresponds to the height of the layer and M is the constant mobility. For the elastic variables, we apply the scalings

$$C_{ijkl} = C^*_{ijkl} \frac{E_{\mathrm{Si}}}{2(1+\nu)}, \quad u_i = u_i^* \alpha H_0, \quad \epsilon_{ij} = \epsilon^*_{ij} \alpha, \quad \sigma_{ij} = \sigma^*_{ij} \frac{\alpha E_{\mathrm{Si}}}{2(1+\nu)}.$$

After dropping the *, the nondimensionalized problem can be written as

$$\partial_t c = \nabla^2 \left(\mu + \varepsilon \beta \, \partial_t c \right), \tag{2.11a}$$

$$\mu = -\varepsilon \nabla^2 c + \frac{1}{\varepsilon} f'(c) + \delta \, \partial_c W(\epsilon_{ij}, c), \tag{2.11b}$$

$$\partial_j \sigma_{ij} = 0, \tag{2.11c}$$

$$\sigma_{ij} = 2G \left(\epsilon_{ij} - \epsilon^0_{ij} \right) + \frac{2\nu}{1-2\nu} G \left(\epsilon_{kk} - \epsilon^0_{kk} \right) \delta_{ij}, \tag{2.11d}$$

where the constitutive laws for the nondimensional shear modulus $G = E(c)/E_{\mathrm{Si}}$ and stress-free strain ϵ^0_{ij} are specified as

$$G = 1 + g(c) \left(\frac{E_{\mathrm{Li_xSi}}}{E_{\mathrm{Si}}} - 1 \right), \quad \epsilon^0_{ij} = h(c),$$

and the derivative of the nondimensional elastic energy takes the form

$$\begin{aligned} \partial_c W(\epsilon_{ij}, c) = {} & \frac{(1-\nu)G'}{1-2\nu} \left(\partial_1 u_1^2 + \partial_2 u_2^2 \right) + \frac{1}{2} G' \left(\partial_1 u_2 + \partial_2 u_1 \right)^2 \\ & + \frac{2\nu G'}{1-2\nu} \partial_1 u_1 \partial_2 u_2 - \frac{2(1+\nu)}{1-2\nu} (h(c)G)' \nabla \cdot \mathbf{u} \\ & + \frac{3(1+\nu)}{1-2\nu} \left(h(c)^2 G \right)'. \end{aligned} \tag{2.11e}$$

Here, $h(c)$ and $g(c)$ are interpolating functions such that $g(0) = h(0) = 0$ and $g(1) = h(1) = 1$. Note that we have slightly generalized our previous choice (2.3) for ϵ^0_{ij}, while letting $\bar{c} = 0$. Also, note that we have not defined a scaling for c, but this should define 0 and 1 to be the two equilibrium concentrations. For the boundaries in contact with the substrate, we will take a no-flux/no-deformation boundary condition:

$$\mathbf{u} = 0, \quad \mathbf{n} \cdot \nabla c = 0, \quad \mathbf{n} \cdot \nabla \mu = 0, \tag{2.11f}$$

where $\mathbf{n}$ is the normal vector to the surface. In the case of the boundaries in contact with the electrolyte, we take a no-traction boundary condition and, following [5], assume a consistent no-flux condition for c (also known as *variational boundary condition*), together with a Butler-Volmer type absorption condition for the chemical potential[32]

$$\sigma \cdot \mathbf{n} = 0, \quad \mathbf{n} \cdot \nabla c = 0, \quad \mathbf{n} \cdot \nabla \mu = K(\mu) = k \left(1 - e^{Q(\mu - \mu_{ext})} \right), \tag{2.11g}$$

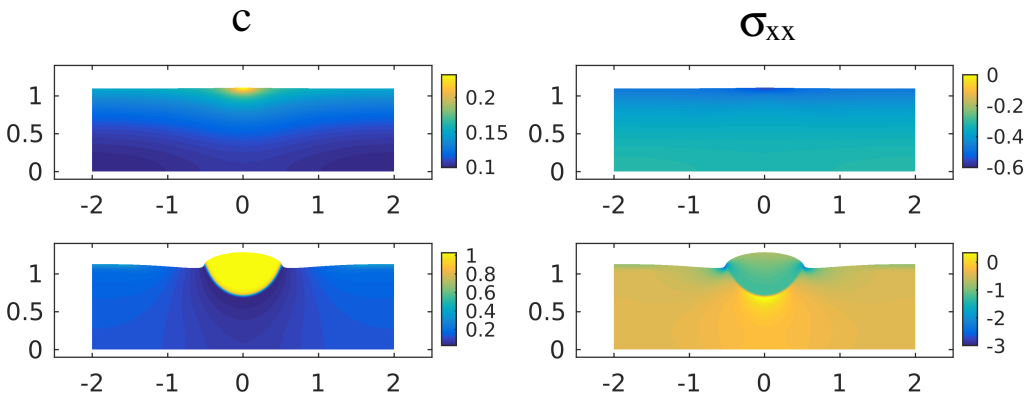

Figure 1: Top: Concentration and σ_{xx} at $t = 0.027$. Bottom: Concentration and σ_{xx} at $t = 0.037$. We use the constant flux boundary condition and the parameters are: $\beta = 0.1$ and $\delta = 0.1$. (nondimensional units, the deformation has been scaled to obtain a better visualization)

where, μ_{ext} is scaled like μ. Apart from this Butler-Volmer-type absorbtion condition we will also consider the constant flux boundary conditions $\mathbf{n} \cdot \nabla \mu = k$.

The problem thus depends on the following non-dimensional groups:

$$\beta = \frac{\chi M}{H_0}, \quad k = \frac{k_r H_0^2}{M\gamma}, \quad \delta = \frac{H_0 E_{\mathrm{Si}} \alpha^2}{2(1+\nu)\gamma}, \quad Q = \frac{\gamma H_0^{-1}}{k_B T}. \tag{2.12}$$

with the elastic ratio $E_{\mathrm{Li_xSi}}/E_{\mathrm{Si}}$ and ν, together with the parameter μ_{ext} and ϵ. Note that Q and k play a similar role in the vicinity of equilibrium, and δ is the ratio of elastic to interfacial energies.

For the numerical simulations we have used $E_{\mathrm{Li_xSi}}/E_{\mathrm{Si}} = 4/9$ and $\nu = 0.25$, in accordance with the calculations form Shenoy et al. [29]. We also use $\epsilon = 0.005$ and $k = 4.0$ except where indicated.

3 Sharp-interface asymptotics

For a typical scenario, where small defects on the free interface lead to preferred absorption sites of the incoming ions, the critical concentration that initiates the phase transition is reached there first and leads to the local formation of sharp phase boundaries and the growth of lithiated regions. In Fig. 1 we show snapshots of such an event (see Section 4 below and Ref. [22] for more information on the numerics). It shows the concentration and σ_{xx} before and after the formation of the sharp interface in the presence of a non-uniform flux. In this case, we have taken the flux in a small region near $x = 0$ to be approximately two times the value outside of it.

On top of Fig. 1 there is a characteristic concentration pattern just before phase separation. Near $x = 0$ the concentration is higher than elsewhere, but this is not so clearly reflected in the stress field, which is more compressive near the top, where the

concentration is the highest. After phase separation takes place and the sharp interface is created we show near the bottom of Fig. 1 the corresponding cross-sections. Now the deformation is much more visible, as we have two distinct phases with concentrations near $c = 1$ and $c = 0$. We see how σ_{xx} is more negative in the transformed phase, indicating a strong compression and this compression is highest near the triple junctions. In this example we have prescribed a constant flux as in [22], and taken lateral periodic boundary conditions for simplicity.

It will be difficult to analyse systematically these nucleation and growth processes, where diffusion, elasticity and interfacial effects are present and hard to disentangle using the present model. However, in the past it has been shown to be instructive to derive reduced sharp-interface models describing the dynamics asymptotically.

To our knowledge, the first development of this kind for a similar problem (an Allen-Cahn equation coupled with nonlinear elasticity) was made by [11]. They did a comprehensive study and developed a Gibbs-Thomson equation that incorporates the right *Eshelby Traction*.

The original reference for the analysis of our problem (i.e. the Larché-Cahn system, understood as a Cahn-Hilliard equation coupled with linear elasticity) is [15]. The authors compare the results with a boundary integral approach and write explicitly the correspondence between the sharp and the diffuse interface models. According to their result, the elastic term in the chemical potential has to have a particular scaling with the interface width in order to recover instantaneous diffusion away from the interface. Also, they find out that for that purpose, the interpolating functions of c that define E and ϵ^0_{ij} must fulfill some conditions.

Further analysis has been performed since then. For instance, [12] proved some existence and uniqueness results for the diffuse interface model, followed by an asymptotic analysis [13], finding the corresponding sharp-interface model. More recently, [1] has proven rigorously these asymptotic results. However, none of these studies consider realistic boundary conditions.

3.1 Sharp-interface in the bulk

3.1.1 Outer Expansion

$$c(x,y,t) = c_0 + \varepsilon c_1 + \varepsilon^2 c_2 + ..., \tag{3.1a}$$

$$\mu(x,y,t) = \varepsilon^{-1}\mu_{-1} + \mu_0 + \varepsilon\mu_1 + ..., \tag{3.1b}$$

$$u_i(x,y,t) = u_{i,0} + \varepsilon u_{i,1} + \varepsilon^2 u_{i,2} + ..., \tag{3.1c}$$

$$\sigma_{ij}(x,y,t) = \varepsilon^{-1}\sigma_{ij,-1} + \sigma_{ij,0} + \varepsilon\sigma_{ij,1} + \varepsilon^2\sigma_{ij,2} + ..., \tag{3.1d}$$

For the Cahn-Hilliard equation we obtain, matching powers of ε

$$\nabla^2\mu_{-1} = 0, \tag{3.2}$$

$$\partial_t c_0 - \nabla^2\mu_0 = 0. \tag{3.3}$$

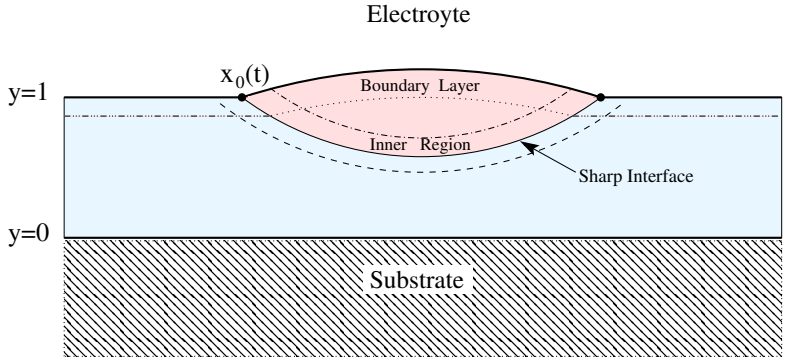

Figure 2: Sketch of the layer. We show in pink the lithiated region and we mark the different regions that require a separate treatment: The inner region, the boundary layer and the triple junction point at $x_0(t)$.

No additional equations are necessary. The values of the chemical potential are:

$$\mu_{-1} = f'(c_0), \tag{3.4}$$
$$\mu_0 = f''(c_0)c_1 + \delta\,\partial_c W(u_{i,0}, c_0). \tag{3.5}$$

Note the dependence of μ_0 on the elastic energy. Interpolating functions $h(c)$ and $g(c)$ can be chosen to avoid these terms. This implies

$$h'(c_0^{\pm}) = G'(c_0^{\pm}) = 0, \tag{3.6}$$

where $c_0^{\pm}$ are the values of c_0 on either side of the interface. We will see below that these are constant, and correspond to minima of F. Hence, together with the requirement that the value of F is at a minimum far from the interface, we obtain that c_0 is a constant and $\mu_{-1} = 0$

The elastic equilibrium equation has the same form to all orders:

$$\nabla \cdot \boldsymbol{\sigma}_m = 0, \tag{3.7}$$

where the index m refers to the order of the expansion. A brief inspection of this equation for $m = -1$ (and anticipation of continuity of $\boldsymbol{\sigma}_{-1}$ across the interface) leads to the conclusion that $\boldsymbol{\sigma}_{-1} = 0$, hence we restrict our attention in the outer solution to $m = 0, 1, \ldots$.

3.1.2 Inner Expansion

For the inner variables near the interface we introduce curvilinear coordinates r and s via the transformations

$$x = X(s,t) + rY'(s,t), \quad y = Y(s,t) - rX'(s,t), \tag{3.8a}$$

with $X'^2 + Y'^2 = 1$, (primes denote differentiation with respect to s) and scale r the coordinate normal to the evolving interface as $r = \varepsilon\,\rho$. In terms of these inner coordinates (ρ, s), the operators can be written in the following form

$$\nabla^2 \to \varepsilon^{-2}\partial_\rho^2 + \varepsilon^{-1}\mathcal{K}\partial_\rho - \rho\,\mathcal{K}^2\partial_\rho + \partial_s^2 + ..., \tag{3.8b}$$

$$\partial_t \to -\frac{v_n}{\varepsilon}\partial_\eta - v_t\,\partial_s + \partial_t + ..., \tag{3.8c}$$

where $\mathcal{K}$ is the curvature of the interface and $v_n = Y'\dot{X} - X'\dot{Y}$ and $v_t = X'\dot{X} + Y'\dot{Y}$ are the normal and tangential interface velocities We denote the inner variables with tilde and introduce asymptotic expansions similarly as for the outer problem

$$\tilde{c}(\rho, s, t) = \tilde{c}_0 + \varepsilon\tilde{c}_1 + \epsilon^2\tilde{c}_2 + ..., \tag{3.9a}$$

$$\tilde{\mu}(\rho, s, t) = \varepsilon^{-1}\tilde{\mu}_{-1} + \tilde{\mu}_0 + \varepsilon\tilde{\mu}_1 + ..., \tag{3.9b}$$

$$\tilde{u}_i(\rho, s, t) = \tilde{u}_{i,0} + \varepsilon\tilde{u}_{i,1} + \varepsilon^2\tilde{u}_{i,2} + ..., \tag{3.9c}$$

$$\tilde{\sigma}_{ij}(\rho, s, t) = \varepsilon^{-1}\tilde{\sigma}_{ij,-1} + \tilde{\sigma}_{ij,0} + \varepsilon\tilde{\sigma}_{ij,1} + \varepsilon^2\tilde{\sigma}_{ij,2} + ..., \tag{3.9d}$$

We start with the first order of the elastic equilibrium equation, Eq. (2.11c). From the formulas of the appendix we obtain, to order ε^{-2}:

$$(\nabla \cdot \boldsymbol{\sigma})_r = \partial_\rho\tilde{\sigma}_{rr,-1} = 0, \tag{3.10a}$$

$$(\nabla \cdot \boldsymbol{\sigma})_s = \partial_\rho\tilde{\sigma}_{rs,-1} = 0, \tag{3.10b}$$

from which follows that

$$G(\tilde{c}_0)\partial_\rho\tilde{u}_{r,0} = A_r, \tag{3.11a}$$

$$G(\tilde{c}_0)\partial_\rho\tilde{u}_{s,0} = A_s, \tag{3.11b}$$

And hence

$$\tilde{u}_{r,0} = A_r\int_0^\rho \frac{1}{G(\tilde{c}_0)}d\rho' + B_r, \tag{3.12a}$$

$$\tilde{u}_{s,0} = A_s\int_0^\rho \frac{1}{G(\tilde{c}_0)}d\rho' + B_s. \tag{3.12b}$$

We will see below that $\tilde{c}_0$ will correspond to a kink-like solution with a bounded range, and $G(\tilde{c}_0)$ is also bounded by construction, as it is constructed as a polynomial function of $\tilde{c}_0$. This implies that both integrals will in general diverge as $\rho \to \infty$, which means in turn that it will be impossible to match to the outer solution unless $A_r = A_s = 0$. This will also make sure that the displacement field is continuous. The previous result implies that

$$\partial_\rho\tilde{u}_{s,0} = \partial_\rho\tilde{u}_{r,0} = 0, \tag{3.13}$$

and therefore

$$\tilde{\sigma}_{rr,-1} = \tilde{\sigma}_{rs,-1} = \tilde{\sigma}_{sr,-1} = 0.$$

The other component of the stress tensor is also zero to this order ($\tilde{\sigma}_{ss,-1} = 0$). Similarly, the strain tensor to this order is also zero.

In the next order, the elastic equations read as follows:

$$\partial_\rho \tilde{\sigma}_{rr,0} = 0, \quad \partial_\rho \tilde{\sigma}_{rs,0} = 0, \tag{3.14}$$

since the lower order term does not contribute. These equations imply that $\tilde{\sigma}_{rr,0}$ and $\tilde{\sigma}_{rs,0}$ do not depend on ρ. Then, the matching condition

$$\lim_{\rho \to \pm\infty} \left(\tilde{\sigma}_{ij,0} - \sigma^{\pm}_{ij,0} \right) = 0, \tag{3.15}$$

implies that $\tilde{\sigma}_{rr,0}$ and $\tilde{\sigma}_{rs,0}$ are continuous. This means that, to zero order, the condition of continuous tractions along the discontinuity is fulfilled. This equation together with the continuity of the displacements ensures a *coherent* interface.

Note that equations (3.14), while giving continuity of the tractions $\boldsymbol{\sigma} \cdot \mathbf{n}$ through the interface, they also imply a jump condition on the derivatives of the displacement field. In terms of the displacement field the equations read as follows:

$$\partial_\rho \left[G(\tilde{c}_0) \left((1-\nu)\partial_\rho \tilde{u}_{r,1} + \nu \left(\partial_s \tilde{u}_{s,0} + \tilde{u}_{r,0}\mathcal{K} \right) - (1+\nu) h(\tilde{c}_0) \right) \right] = 0, \tag{3.16a}$$

$$\partial_\rho \left[G(\tilde{c}_0) \left(\partial_s \tilde{u}_{r,0} + \partial_\rho \tilde{u}_{s,1} - \mathcal{K}\tilde{u}_{s,0} \right) \right] = 0. \tag{3.16b}$$

These equations can be integrated once and then matched term by term to the outer solution, here given in terms of curvilinear coordinates

$$G(c_0^{\pm}) \left((1-\nu)\partial_r u^{\pm}_{r,0} + \nu \left(\partial_s u_{s,0} + u_{r,0}\mathcal{K} \right) - (1+\nu) h(c_0^{\pm}) \right) = K_1(s), \tag{3.17a}$$

$$G(c_0^{\pm}) \left(\partial_s u_{r,0} + \partial_r u^{\pm}_{s,0} - \mathcal{K} u_{s,0} \right) = K_2(s). \tag{3.17b}$$

By subtracting the negative limit from the positive limit we obtain a closed jump condition for the normal derivatives of the displacement field. Once we have found the continuity of $u_{i,0}$ and the continuity of tractions for $\sigma_{ij,0}$, we move on to the Cahn-Hilliard equation. We start by writing down explicitly the form of the chemical potential, by including also the terms coming from Eq. (A.20) of the Appendix:

$$\tilde{\mu}_{-1} = -\partial_\rho^2 \tilde{c}_0 + f'(\tilde{c}_0), \tag{3.18a}$$

$$\begin{aligned} \tilde{\mu}_0 = {} & -\mathcal{K}\partial_\rho \tilde{c}_0 + f''(\tilde{c}_0)\tilde{c}_1 - \partial_\rho^2 \tilde{c}_1 \\ & + \frac{\delta}{2} \left[-2h'(\tilde{c}_0)\delta_{ij}\tilde{\sigma}_{ij,0} + \frac{G'(\tilde{c}_0)}{G(\tilde{c}_0)} \left(\tilde{\epsilon}_{ij,0} - h(\tilde{c}_0)\delta_{ij} \right) \tilde{\sigma}_{ij,0} \right], \end{aligned} \tag{3.18b}$$

$$\begin{aligned} \tilde{\mu}_1 = {} & \rho\mathcal{K}^2\partial_\rho \tilde{c}_0 - \partial_s^2 \tilde{c}_0 - \mathcal{K}\partial_\rho \tilde{c}_1 + \frac{1}{2} f'''(\tilde{c}_0)\tilde{c}_1^2 + f''(\tilde{c}_0)c_2 - \partial_\rho^2 c_2 \\ & + \frac{\delta}{2} \left[-2 \left(h'(\tilde{c}_0)\delta_{ij}\sigma_{ij,1} + h''(\tilde{c}_0)\tilde{c}_1\delta_{ij}\tilde{\sigma}_{ij,0} \right) + \frac{G'(\tilde{c}_0)}{G(\tilde{c}_0)} \left(\tilde{\epsilon}_{ij,1} - h'(\tilde{c}_0)\tilde{c}_1\delta_{ij} \right) \tilde{\sigma}_{ij,0} \right. \\ & \left. + \frac{G'(\tilde{c}_0)}{G(\tilde{c}_0)} \left(\tilde{\epsilon}_{ij,0} - h(\tilde{c}_0)\delta_{ij} \right) \sigma_{ij,1} + \frac{G''(\tilde{c}_0)G(\tilde{c}_0) - G'(\tilde{c}_0)^2}{G(\tilde{c}_0)^2} \tilde{c}_1 \left(\epsilon_{ij,0} - h(\tilde{c}_0)\delta_{ij} \right) \tilde{\sigma}_{ij,0} \right], \end{aligned} \tag{3.18c}$$

note that for $\tilde{\mu}_0$ and $\tilde{\mu}_1$ we only write the non-zero elastic terms. Also notice that the derivative of the elastic energy might bring terms of order ϵ^{-2} to the chemical potential, but they all cancel. This can be easily checked by expanding Eq. (A.20) in the appendix and using Eq. (3.13) We now proceed order by order with the Cahn-Hilliard equation:

Order ε^{-3} To this order, the Cahn-Hilliard equation reads

$$\partial_\rho^2 \tilde{\mu}_{-1} = 0. \tag{3.19}$$

This means that from Eq. (3.18a) we have:

$$\partial_\rho^2 \left(-\partial_\rho^2 \tilde{c}_0 + f'(\tilde{c}_0)\right) = 0. \tag{3.20}$$

Following the usual assumptions [27] and making $\tilde{\mu}_{-1}$ a constant, we take a traveling-wave solution of the problem $\tilde{c}_0(\rho)$ such that

$$\lim_{\eta \to \pm\infty} \tilde{c}_0(\rho) = c_0^{\pm}, \tag{3.21}$$

i.e. it has two constant limits that match the outer solution, implying that the latter is constant. If we assume that far from the interface the system is in one of the homogeneous equilibria, then $\mu_{-1} = 0$ will be the outer solution with the right boundary conditions. This also implies $\tilde{\mu}_{-1} = 0$.

Order ε^{-2} To this order the Cahn-Hilliard equation reads

$$\mathcal{K}\partial_\rho \tilde{\mu}_{-1} - \beta v_n \partial_\rho^3 \tilde{c}_0 + \partial_\rho^2 \tilde{\mu}_0 = 0. \tag{3.22}$$

The first term is zero and the last term can be expanded following Eq. (3.18b):

$$-\beta v_n \partial_\rho^3 \tilde{c}_0 + \partial_\rho^2 \left(-\mathcal{K}\partial_\rho \tilde{c}_0 + f''(\tilde{c}_0)\tilde{c}_1 - \partial_\rho^2 \tilde{c}_1 + \delta\, \partial_{\tilde{c}} \tilde{W}(\tilde{\boldsymbol{\epsilon}}, \tilde{c})_0\right) = 0, \tag{3.23}$$

with the obvious shorthand

$$\partial_{\tilde{c}} \tilde{W}(\tilde{\boldsymbol{\epsilon}}, \tilde{c})_0 = \frac{1}{2}\left[-2h'(\tilde{c}_0)\delta_{ij}\tilde{\sigma}_{ij,0} + \frac{G'(\tilde{c}_0)}{G(\tilde{c}_0)}\left(\tilde{\epsilon}_{ij,0} - h(\tilde{c}_0)\delta_{ij}\right)\tilde{\sigma}_{ij,0}\right]. \tag{3.24}$$

Eq. (3.23) can be integrated twice to yield:

$$-\beta v_n \partial_\rho \tilde{c}_0 - \mathcal{K}\partial_\rho \tilde{c}_0 + f''(\tilde{c}_0)\tilde{c}_1 - \partial_\rho^2 \tilde{c}_1 + \delta\, \partial_{\tilde{c}} \tilde{W}(\tilde{\boldsymbol{\epsilon}}, \tilde{c})_0 = A\rho + B, \tag{3.25}$$

with A and B being constants. By matching with the outer solution:

$$\lim_{\rho \to \pm\infty} (\tilde{c}_1 - c_1 - \rho \partial_r c_0) = 0, \tag{3.26}$$

and since in curvilinear coordinates, $\partial_r c_0 = 0$, it follows that $\tilde{c}_1$ is bounded if c_1 is bounded as $\rho \to \pm\infty$, and hence $A = 0$ since all the other elements on the LHS of (3.25) are bounded as $\rho \to \pm\infty$ (we have used implicitly Eq. (3.6) to show that the elastic

terms do not contribute). Alternatively, one can deduce the previous result by matching $\tilde{\mu}_0 - \beta\partial_\rho\tilde{c}_0$ to their outer counterparts. Since $\partial_\rho c_0^\pm = \partial_r \mu_{-1}^\pm = 0$ we obtain the desired result. To obtain the constant B, equal to $\tilde{\mu}_0 - \beta v_n \partial_\rho \tilde{c}_0$, we notice the following. Eq. (3.25) has the form

$$f''(\tilde{c}_0)\tilde{c}_1 - \partial_\rho^2 \tilde{c}_1 = \mathcal{G}. \tag{3.27}$$

It is easy to prove that $\partial_\rho \tilde{c}_0$ is a solution of the homogeneous problem. Since the operator is self-adjoint, because of the Fredholm alternative we obtain the following solvability condition:

$$\int_{-\infty}^{\infty} \partial_\rho \tilde{c}_0 \, \mathcal{G} \, d\rho = 0 \tag{3.28}$$

This means that

$$(\beta\, v_n + \mathcal{K}) \int_{-\infty}^{+\infty} (\partial_\rho \tilde{c}_0)^2 \, d\rho - \delta \int_{-\infty}^{+\infty} \partial_\rho \tilde{c}_0 \partial_{\tilde{c}} \tilde{W}(\tilde{\boldsymbol{\epsilon}}, \tilde{c})_0 \, d\rho + B(c_0^+ - c_0^-) = 0. \tag{3.29}$$

Since $\partial_\rho \tilde{c}_0$ goes to zero as $\rho \to \pm\infty$, B matches μ_0. The first integral can be readily performed, but the second one requires a more careful analysis. First, we observe that

$$W^+ - W^- = \int_{-\infty}^{+\infty} \partial_\rho \tilde{c}_0 \, \partial_{\tilde{c}_0} \tilde{W}(\tilde{\boldsymbol{\epsilon}}_0, \tilde{c}_0) \, d\rho + \int_{-\infty}^{+\infty} d\rho \partial_\rho \tilde{\epsilon}_{ij,0} \partial_{\tilde{\epsilon}_{ij,0}} \tilde{W}(\tilde{\boldsymbol{\epsilon}}_0, \tilde{c}_0), \tag{3.30}$$

which can be obtained from the total derivative of $\tilde{W}$ with respect to ρ (note that $\partial_{\tilde{c}} \tilde{W}(\tilde{\boldsymbol{\epsilon}}, \tilde{c})_0 = \partial_{\tilde{c}_0} \tilde{W}(\tilde{\boldsymbol{\epsilon}}_0, \tilde{c}_0)$). We observe that the first integral is the one that we are interested in, and the second once can be readily computed. First we notice that

$$\int_{-\infty}^{+\infty} \partial_\rho \tilde{\epsilon}_{ij,0} \, \partial_{\tilde{\epsilon}_{ij,0}} \tilde{W}(\tilde{\boldsymbol{\epsilon}}_0, c_0) \, d\rho = \int_{-\infty}^{+\infty} \partial_\rho \tilde{\epsilon}_{ij,0} \, \tilde{\sigma}_{ij,0} \, d\rho. \tag{3.31}$$

The sum runs over all indices except ss, since this component does not depend on ρ, see Appendix B. By integrating by parts we have that

$$\int_{-\infty}^{+\infty} \partial_\rho \tilde{\epsilon}_{ij,0} \, \tilde{\sigma}_{ij,0} \, d\rho = [\epsilon_{ij,0}\sigma_{ij,0}]_\pm - \int_{-\infty}^{+\infty} \tilde{\epsilon}_{ij,0} \, \partial_\rho \tilde{\sigma}_{ij,0} \, d\rho, \tag{3.32}$$

but the last integral is zero because of Eqs. (3.14) (note again that the sum excludes $i = s$ and $j = s$). By using the continuity of all $\sigma_{ij,0}$ except $\sigma_{ss,0}$ and because of the continuity of $\epsilon_{ss,0}$ we can write more compactly:

$$\int_{-\infty}^{+\infty} \partial_\rho \tilde{c}_0 \, \partial_{\tilde{c}_0} \tilde{W}(\tilde{\boldsymbol{\epsilon}}_0, \tilde{c}_0) \, d\rho = W^+ - W^- - \sigma_{ij,0}^+ \left(\epsilon_{ij,0}^+ - \epsilon_{ij,0}^- \right), \tag{3.33}$$

where the sum runs over all indices.

Hence, we obtain the following boundary condition:

$$\begin{aligned} \mu_0^\pm (c_0^+ - c_0^-) = &- (\beta\, v_n + \mathcal{K})\, I + \frac{\delta}{2} \left[\sigma_{ij,0}^+ \left(\epsilon_{ij,0}^+ - \delta_{ij} h(c_0^+) \right) - \sigma_{ij,0}^- \left(\epsilon_{ij,0}^- - \delta_{ij} h(c_0^-) \right) \right] \\ &- \delta \sigma_{ij,0}^+ \left(\epsilon_{ij,0}^+ - \epsilon_{ij,0}^- \right), \end{aligned} \tag{3.34}$$

where I is the integral in (3.29). This same formula without the kinetic term is found in [15]. The last term corresponds to the elastic energy required to maintain coherence at the interface [17, 16].

Order ε^{-1} To this order the Cahn-Hilliard equation reads as follows:

$$-v_n\partial_\rho\tilde{c}_0 = \mathcal{K}\partial_\rho\tilde{\mu}_0 - \beta\, v_n\partial_\rho^3\tilde{c}_1 + \partial_\rho^2\tilde{\mu}_1 - \beta\,\partial_\rho^2\left(v_t\partial_s\tilde{c}_0 - \partial_t\tilde{c}_0\right) - \beta\, v_n\mathcal{K}\partial_\rho^2\tilde{c}_0, \tag{3.35}$$

where we have used explicitly $\tilde{\mu}_{-1} = 0$. We can integrate the previous equation once:

$$-v_n\tilde{c}_0 = \mathcal{K}\tilde{\mu}_0 - \beta\, v_n\partial_\rho^2\tilde{c}_1 + \partial_\rho\tilde{\mu}_1 - \beta\,\partial_\rho\left(v_t\partial_s\tilde{c}_0 - \partial_t\tilde{c}_0\right) - \beta\, v_n\mathcal{K}\partial_\rho\tilde{c}_0 + C, \tag{3.36}$$

where C is and integration constant, possibly dependent on s. We can take the limit and match the previous equation term by term to the outer solution in the usual way. We obtain, after taking the limit:

$$-v_n c_0^{\pm} = \partial_r\mu_0^{\pm} + C, \tag{3.37}$$

where all the terms match to zero or to constants independent of the side of the interface, hence the redefinition of C. From here it is immediate to obtain the conservation condition:

$$\left(c_0^+ - c_0^-\right)v_n = -\left(\partial_r\mu_0^+ - \partial_r\mu_0^-\right). \tag{3.38}$$

3.2 Asymptotic analysis near the absorption boundary

In the following we will assume that the boundary is at $y = 1$ and we define an inner coordinate next to the boundary as

$$\eta = \frac{y-1}{\varepsilon}, \tag{3.39}$$

and expand

$$\hat{c}(x,\eta,t) = \hat{c}_0 + \varepsilon\hat{c}_1 + \epsilon^2\hat{c}_2 + ..., \tag{3.40a}$$
$$\hat{\mu}(x,\eta,t) = \varepsilon^{-1}\hat{\mu}_{-1} + \hat{\mu}_0 + \varepsilon\hat{\mu}_1 + ..., \tag{3.40b}$$
$$\hat{u}_i(x,\eta,t) = \hat{u}_{i,0} + \varepsilon\hat{u}_{i,1} + \varepsilon^2\hat{u}_{i,2} + ..., \tag{3.40c}$$
$$\hat{\sigma}_{ij}(x,\eta,t) = \hat{\sigma}_{ij,0} + \varepsilon\hat{\sigma}_{ij,1} + \varepsilon^2\hat{\sigma}_{ij,2} + ... \tag{3.40d}$$

The first two orders for (2.11a) in inner coordinates at the boundary are

$$\partial_\eta^2\hat{\mu}_{-1} = 0, \tag{3.41a}$$
$$\partial_\eta^2\hat{\mu}_0 = 0, \tag{3.41b}$$

Remarkably, the third condition (2.11g) brings in terms to all negative orders when $\hat{\mu}_{-1}$ is not zero at the boundary. These would be impossible to match unless $\tilde{\mu}_{-1}$ is zero at the boundary. Hence we have this boundary condition, together with the matching to the outer solution:

$$\lim_{\eta\to-\infty}\hat{\mu}_{-1} = \mu_{-1} = 0.$$

Together with (3.41a), this implies that

$$\hat{\mu}_{-1} = 0. \tag{3.42}$$

The boundary condition for (3.41b) then is

$$\partial_\eta \hat{\mu}_0 = 0, \tag{3.43}$$

as once $\hat{\mu}_{-1} = 0$ there are no $O(\varepsilon^{-1})$ terms in the right hand side of (2.11g). It follows that the solution of Eq. (3.41b) is a constant with respect to η, $\hat{\mu}_0 = \hat{\mu}_0(x)$, Thus $\hat{\mu}_0(x)$ is determined by the outer solution via matching, $\mu_{y=1} = \hat{\mu}_0(x)$, rather than vice-versa.

Notice that rescaling (2.11d) to inner coordinates introduces terms of order ϵ^{-1}. However, if we include terms to this order in the expansion (3.40d) for $\hat{\sigma}_{ij}$, they lead to homogeneous problems for the components of σ both for the PDE and the boundary value problems, leading to a trivial solution. Hence, the terms of order ϵ^{-1} in the expansion of (2.11d) have to vanish as well, which implies that

$$\partial_\eta \hat{u}_{1,0} = 0, \quad \partial_\eta \hat{u}_{2,0} = 0. \tag{3.44}$$

Order $\boldsymbol{\varepsilon^{-1}}$. To this order, (2.11) becomes

$$\partial_\eta^2 \hat{\mu}_1 + \partial_x^2 \hat{\mu}_{-1} = 0, \tag{3.45a}$$

$$\hat{\mu}_{-1} = -\partial_\eta^2 \hat{c}_0 + f'(\hat{c}_0), \tag{3.45b}$$

$$\partial_\eta \hat{\sigma}_{iy,0} = 0, \qquad i = x, y. \tag{3.45c}$$

where $\hat{\mu}_{-1} = 0$. The first of these implies that $\partial_\eta \hat{\mu}_1$ does not depend on η. The boundary condition for $\hat{\mu}_1$ gives

$$\partial_\eta \hat{\mu}_1 = k\left(1 - e^{Q(\mu_0 - \mu_{ext})}\right). \tag{3.46}$$

Using the matching condition

$$\lim_{\eta \to -\infty} \left(\partial_\eta \hat{\mu}_1 - \partial_y \mu_0|_{y=1}\right) = 0, \tag{3.47}$$

leads to

$$\partial_y \mu_0|_{y=1} = k\left(1 - e^{Q(\mu_0 - \mu_{ext})}\right), \tag{3.48}$$

that is, $\tilde{\mu}_0$ inherits the boundary condition from the full problem.

Regarding the concentration, (3.45b) has to be fulfilled. Notice that no contribution of $\partial_c W$ appears in this equation, as the possible $O(\epsilon^{-1})$ (and, as matter of fact, $O(\epsilon^{-2})$) contributions vanish due to (3.44). For (3.45b), we have on the one hand that

$$\lim_{\eta \to -\infty} \hat{c}_0 = c^{\pm},$$

and on the other $\partial_\eta \hat{c}_0|_{\eta=0} = 0$, which rules out kink-like solutions. This implies that

$$\hat{c}_0 = c^{\pm}. \tag{3.49}$$

Integrating (3.45c), and using the $O(1)$ approximation of the boundary condition for $\hat{\boldsymbol{\sigma}}$ from (2.11g) in inner coordinates, we obtain $\hat{\sigma}_{iy,0} = 0$ for $i = x, y$. Matching then gives the boundary condition

$$\sigma_{iy,0}|_{y=1} = 0, \quad i = x, y, \tag{3.50}$$

for the outer problem for $\boldsymbol{\sigma}_0$.

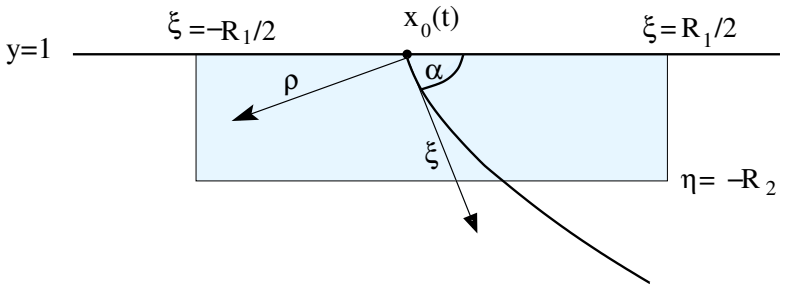

Figure 3: Sketch of coordinate system around a triple point

3.3 Conditions at triple points

We now consider a point where the interface between the two phases meets the boundary of the Silicon domain with the electrolyte following the approach used by [26]. For the boundary located at $y = 1$ so that the layer lies in the region $y < 1$, the triple point is assumed to have the coordinates $x = x_0$ and $y = 1$. We thus rescale according to inner scalings in both Cartesian coordinate directions

$$\xi = \frac{x - x_0(t)}{\varepsilon}, \qquad \eta = \frac{y - 1}{\varepsilon}. \tag{3.51}$$

Rescaling (2.11) gives

$$\varepsilon^2 \partial_t \check{c} - \varepsilon \dot{x}_0 \partial_\xi \check{c} = \nabla^2_{\xi,\eta} \check{\mu}, \tag{3.52a}$$

$$\varepsilon \check{\mu} = -\nabla^2_{\xi,\eta} \check{c} + f'(\check{c}), \tag{3.52b}$$

where $\nabla^2_{\xi,\eta} = \partial^2_\xi + \partial^2_\eta$. Th leading order problem is:

$$\nabla^2_{\xi,\eta} \check{\mu}_0 = 0, \tag{3.53a}$$

$$-\nabla^2_{\xi,\eta} \check{c}_0 + f'(\check{c}_0) = 0. \tag{3.53b}$$

The rescaled boundary conditions at $\eta = 1$ are

$$\partial_\eta \check{c} = 0, \qquad \partial_\eta \check{\mu} = \varepsilon k \left(1 - e^{Q(\check{\mu} - \mu_{ext})}\right), \tag{3.54}$$

thus, to leading order

$$\partial_\eta \check{c}_0 = 0, \qquad \partial_\eta \check{\mu}_0 = 0, \tag{3.55}$$

at $\eta = 1$. Notice that the flux from the Butler-Vollmer condition has dropped out and the problem (3.52), (3.55) is the same problem that has been considered for the triple point at a solid wall elsewhere in the literature, e.g. [3]. We summarise the key arguments in the following to recover that the interface between the phases meets the boundary with the electrolyte orthogonally

Multiply (3.53b) with $\partial_\xi \check{c}_0$ and integrate over the box $R \equiv [-R_1/2, R_1/2] \times [-R_2, 0]$, to get

$$\iint_R f'(\check{c}_0)\, \partial_\xi \check{c}_0 \, d\eta d\rho = \iint_R \partial_\xi \check{c}_0 \nabla^2_{\xi,\eta} \check{c}_0 \, d\eta d\rho, \tag{3.56}$$

or

$$\iint_R f'(\check{c}_0) \partial_\xi \check{c}_0 - \partial_\xi \check{c}_0 \partial^2_\xi \check{c}_0 + \partial_\eta \check{c}_0 \partial_{\xi\eta} \check{c}_0 \, d\eta d\rho = \iint_R \partial_\xi \check{c}_0 \partial^2_\eta \check{c}_0 + \partial_\eta \check{c}_0 \partial_{\xi\eta} \check{c}_0 \, d\eta d\rho. \tag{3.57}$$

We know investigate the left hand side (LHS) and right hand side (RHS) of the last equation separately,

$$\text{LHS} = \int_{-R_2}^{0} \left[f(\check{c}_0) - \frac{1}{2}(\partial_\xi \check{c}_0)^2 + \frac{1}{2}(\partial_\eta \check{c}_0)^2 \right]_{\xi=-R_1/2}^{R_1/2} d\eta. \tag{3.58}$$

Taking R_1 and $R_2 \to \infty$ and using that $\partial_\xi \check{c}_0 \to 0$ for $R_1 \to \pm\infty$, we obtain

$$\lim_{R_1,R_2\to\infty} \text{LHS} = \int_{-\infty}^{0} \lim_{R_1\to\infty} \left[f(\check{c}_0) + \frac{1}{2}(\partial_\eta \check{c}_0)^2 \right]_{\xi=-R_1/2}^{R_1/2} d\eta. \tag{3.59}$$

As $\xi \to \pm\infty$, the solution $\check{c}_0$ has to converge to the boundary layer solution at the boundary with the electrolyte, which are the same for both limits except for a change in sign. This, however, does not affect the value of the expression in the square brackets, so in the limit $R_1 \to \infty$ the contributions at $\xi = R_1/2$ and $\xi = -R_1/2$ cancel out, and

$$\lim_{R_1,R_2\to\infty} \text{LHS} = 0. \tag{3.60}$$

For the right hand side, we have

$$\text{RHS} = \int_{-R_1/2}^{R_1/2} \left[\partial_\xi \check{c}_0 \, \partial_\eta \check{c}_0 \right]_{\eta=-R_2}^{0} d\xi = \int_{-R_1/2}^{R_1/2} \partial_\xi \check{c}_0 \, \partial_\eta \check{c}_0 \Big|_{\eta=-R_2} d\xi, \tag{3.61}$$

where we have used (3.55) at $\eta = 1$. We now introduce a rotated coordinate system that is aligned with the interface between the phases, and denote the angle at which this interface meets the boundary with the electrolyte by α. The aim is of course to determine α through the matching. The new coordinates are

$$\begin{aligned} \rho &= -\xi \sin\alpha - \eta \cos\alpha \\ \varsigma &= \xi \cos\alpha - \eta \sin\alpha, \end{aligned}$$

and this gives

$$\text{RHS} = -\int_{\frac{R_1}{2}\sin\alpha + R_2\cos\alpha}^{-\frac{R_1}{2}\sin\alpha + R_2\cos\alpha} S d\rho \tag{3.62}$$

with

$$S = \cos\alpha \left((\partial_\rho \check{c}_0)^2 - (\partial_\varsigma \check{c}_0)^2 \right) + \left(\frac{\sin^2\alpha - \cos^2\alpha}{\sin\alpha} \right) \partial_\rho \check{c}_0 \, \partial_\varsigma \check{c}_0. \tag{3.63}$$

Now, $\partial_\varsigma \check{c}_0 \to 0$ as $\varsigma \to \infty$, and thus

$$\lim_{R_1,R_2\to\infty} \text{RHS} = \lim_{a\to\infty} \overset{*}{\lim_{R_1,R_2\to\infty}} \int_{\frac{R_1}{2}\sin\alpha+R_2\cos\alpha}^{-\frac{R_1}{2}\sin\alpha+R_2\cos\alpha} -S\, d\rho, \tag{3.64}$$

where $\lim^*$ is taken under the condition that $|R_1\cos\alpha + R_2\sin\alpha| < a$,

$$\lim_{R_1,R_2\to\infty} \text{RHS} = -\cos\alpha \int_{-\infty}^{\infty} \partial_\rho \check{c}_0^2\, d\rho. \tag{3.65}$$

Equating the limits (3.60) and (3.65) and using that the integral in (3.65) is positive, we obtain $\cos\alpha = 0$ i. e. $\alpha = \pi/2$, as expected.

3.4 Sharp-interface model

In summary the complete sharp-interface model can be written as follows:

$$\nabla^2 \mu_0 = 0, \tag{3.66a}$$
$$\nabla \cdot \boldsymbol{\sigma}_0 = 0, \tag{3.66b}$$

together with the constitutive relation for stress:

$$\sigma_{ij,0} = 2G^\pm \left(\epsilon_{ij,0} - \epsilon_{ij}^{0,\pm}\right) + \frac{2\nu}{1-2\nu} G^\pm \left(\epsilon_{kk,0} - \epsilon_{kk}^{0,\pm}\right)\delta_{ij}, \tag{3.66c}$$

where $G^\pm = G(c_0^\pm)$ and $\epsilon_{ij}^{0,\pm} = h(c_0^\pm)$ are constants. The boundary conditions for the elasticity equation correspond to continuity for the elastic field and for the tractions:

$$\mathbf{u}_0^+ = \mathbf{u}_0^-, \tag{3.66d}$$
$$\mathbf{n}\cdot\boldsymbol{\sigma}_0^+ = \mathbf{n}\cdot\boldsymbol{\sigma}_0^-. \tag{3.66e}$$

For the chemical potential equation we have at the interface away from the boundary:

$$\begin{aligned}\mu_0^\pm (c_0^+ - c_0^-) = &-(\beta\, v_n + \mathcal{K})\, I + \frac{\delta}{2}\left[\sigma_{ij,0}^+ \left(\epsilon_{ij,0}^+ - \delta_{ij} h(c_0^+)\right) - \sigma_{ij,0}^- \left(\epsilon_{ij,0}^- - \delta_{ij} h(c_0^-)\right)\right] \\ &- \delta\, \sigma_{ij,0}^+ \left(\epsilon_{ij,0}^+ - \epsilon_{ij,0}^-\right),\end{aligned} \tag{3.66f}$$

$$\left(c_0^+ - c_0^-\right) v_n = -\left(\partial_r \mu_0^+ - \partial_r \mu_0^-\right), \tag{3.66g}$$

where $I = \int_{-\infty}^{+\infty} (\partial_\rho \tilde{c}_0)^2\, d\rho$. For the conditions at the absorbtion boundary we have:

$$\partial_y \mu_0|_{y=1} = k\left(1 - e^{Q(\mu_0 - \mu_{ext})}\right), \tag{3.66h}$$
$$\sigma_{iy,0}|_{y=1} = 0, \quad i = x, y, \tag{3.66i}$$

and at the triple points the angle is $\alpha = \pi/2$.

Note that in the case of constant flux boundary conditions we would obtain the same results, except for the exponential in Eq. (3.66h), that would not be present.

4 Comparisons to phase-field simulations

We now compare the longtime behaviour of the phase-field model (2.11) with the predictions of the sharp-interface model (3.66). In particular, we are interested in the convergence of the sharp-interface solution to the profile of the chemical potential as a function of the interface thickness ε. For that purpose we have computed numerically the solution of the phase-field model in the one-dimensional case. We have used the constant flux boundary condition, and the simulations have been solved using a nonlinear adaptive multigrid algorithm [31]. For details on the simulations see [22].

Fig. 4 summarizes the effect of parameters β and δ on the convergence. The solutions of the sharp interface model to leading order in μ are straight lines in one dimension, meeting at the interface. We show in this figure with dashed lines the straight lines fitted to μ far enough from the inner region, but not too close to the outer boundaries, by using a heuristic algorithm. On top, we see that the value of ε and the value of δ have a strong effect on the quality of the fit. On the one hand, for the smaller value of δ we obtain the expected result, i.e. the inner region becomes narrower with smaller values of ε and the convergence improves, this improvement of the convergence is also reflected in the value of μ at $y = 1$. On the other hand, for $\delta = 10.0$ we see how, while there appears to be some convergence, the solution curves are far from being straight lines. This of course indicates that the sharp interface model is far from valid for such high values of the parameter δ, and a much smaller ε is needed to observe convergence.

On Fig. 4 bottom we see the effect of β. For the higher value of β we have a good convergence, and the inner region becomes narrower as ε decreases. Nevertheless, the effect of β is clear, in that there is a depression near the point where both dashed lines meet. We believe that this is well represented by the expansion in the inner region. Indeed, in the inner expansion, the Cahn-Hilliard equation contains at order ϵ^{-2} a source term proportional to β (see Eq. 3.22), and hence this result is to be expected. For $\beta = 0.01$, the smallest value, we see how this depression in the inner region has disappeared and the agreement with the linear fits is extremely good.

In Fig. 5 we quantify how good is the agreement between the sharp interface and the phase field model by using a sharp interface relation, Eq. (3.66g), and computing how well it is approximated by the quantities extracted from the phase field. We compute the gradients of the chemical potential from the fitting lines in Fig. 4 and compute the velocity of the advancing front also numerically. The ratio of the jump in the derivative and the velocity should be equal to one. We represent the results for $\beta = 0.01$ and $\beta = 0.1$ and the agreement is very good. The parabola that fits the $\beta = 0.01$ case also gives a very good approximation to the $\beta = 0.1$ case, except for the highest value of ε, and has a crossing point with the vertical axis at $\varepsilon = 0$ with a value of 1.00028.

This very good agreement and the quadratic convergence seem to indicate, in accordance with similar results in other systems, e.g. Ref. [23], that the smallest order of the finite ε corrections to Eq. (3.66g) will be $O(\varepsilon^2)$.

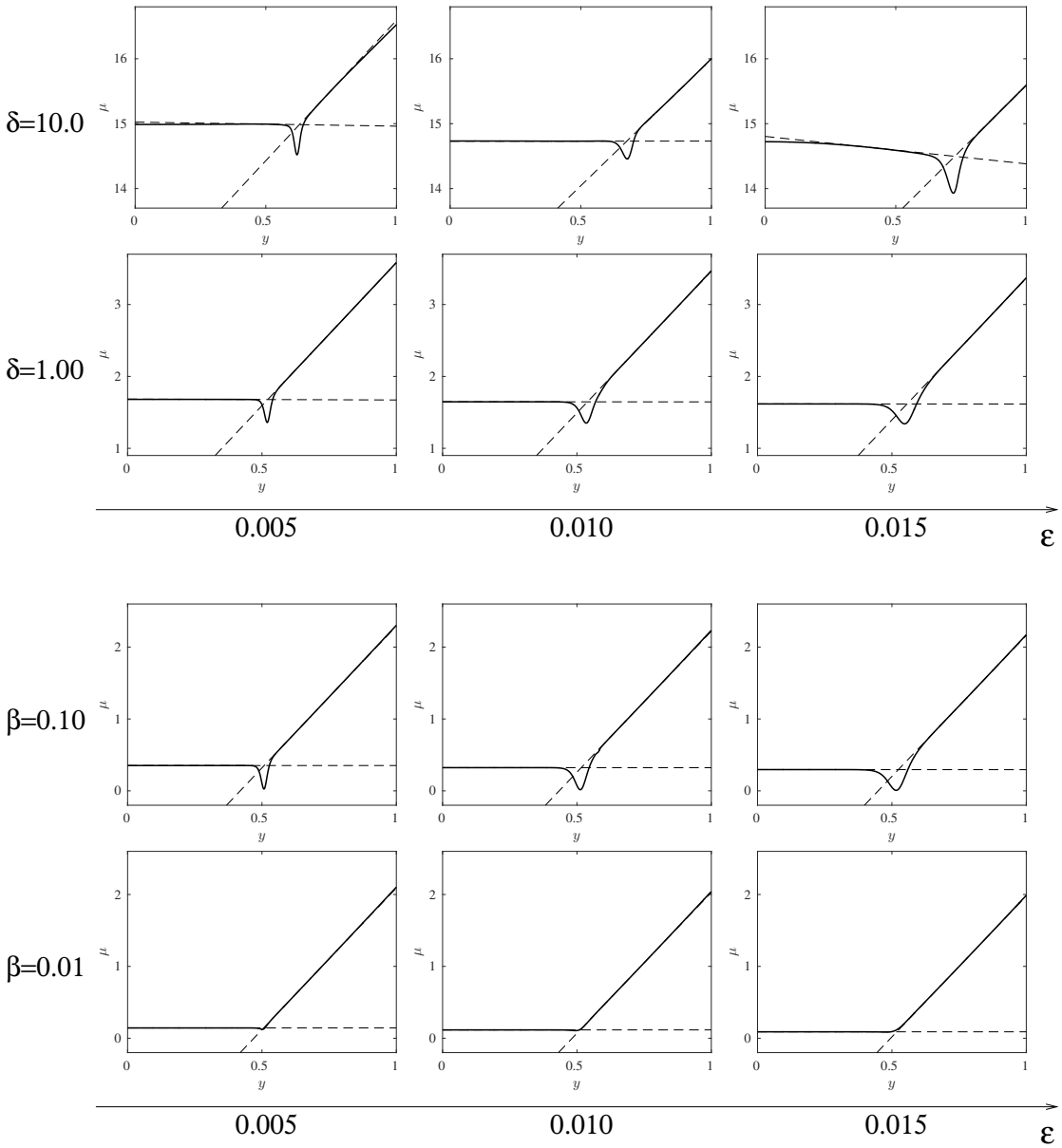

Figure 4: Convergence to the sharp interface limit. Solid lines correspond to the chemical potential μ on the layer, dashed lines correspond to a linear fit near the interface to compute the derivatives. Top: Results for two values of δ. With fixed flux boundary conditions, $\beta = 0.01$ (nondimensional units). Bottom: Results for two values of the kinetic parameter β. With fixed flux boundary conditions, $\delta = 0.1$ (nondimensional units).

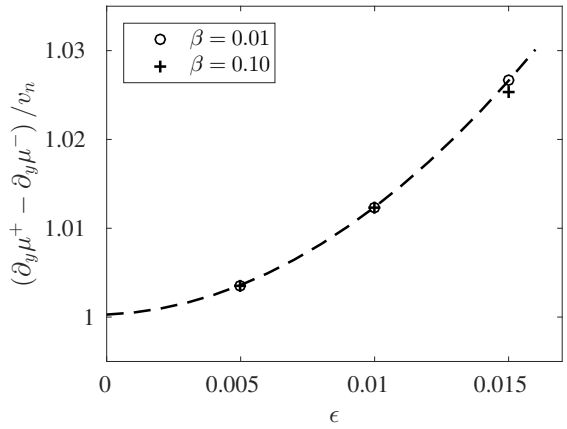

Figure 5: Convergence to the sharp interface limit, for two values of the kinetic parameter β. Symbols correspond to the ratio of the expected velocity to the measured front velocity. The dashed line is a parabolic fit to the $\beta = 0.01$ symbols. With fixed flux boundary conditions, $\delta = 0.1$. (nondimensional units)

5 Conclusion

Understanding the conditions that cause the deformation and eventual destruction of silicon electrode particles during intercalation is a prerequisite to optimizing design and loading conditions. In this regard it is interesting to be able to follow the structure formation and thus the nonuniform stress evolution of a silicon electrode particle in detail and on long time scales as a function of the control parameters, such as the ion flux rate or the ratio of elastic to interfacial energies. In particular, the sharp-interface model we have derived in this study allows for more analytical insight into the complex intercalation process and except for extreemly low lithiation rates, the time scale on which the sharp-interface dynamics takes place is the relevant time scale for comparison with experimental results on the lithiation process.

Results of the comparison of the long-time dynamics of the phase-field model and the velocity deduced from the sharp interface model show a good quadratic convergence, in particular for moderate values of the ratio of elastic to interfacial energies. These are encouraging results, and provide a means to validate the range of parameters in which the phase-field model gives physically robust results.

Natural extensions of this work will include the stabilty of the moving lithiation front and the coarsening mechanisms of the evolving structures. Regarding a more realistic model we note that effects of charge and electrical potential will have to be included in our model, as at this stage our aim was first to understand the role of non-homogeneous elasticity in the stress-lithiation curve, see [22]. In addition, we note that one should be aware of the fact that the underlying phase-field model is only applicable for regimes that depart little from equilibrium, and we are actually considering non-equilibrium phase transitions between what can be at best characterized as metastable states.

As of now, comparisons to experiments can only be qualitative since, as we have mentioned before, we have made the simplified assumption of linear elasticity. However, it will be straight-forward but rather elaborate to include finite strain effects and this is planned for our upcoming research.

Acknowlegements

This research was carried out in the framework of MATHEON supported by Einstein Foundation Berlin.

A Curvilinear Coordinates

Change of coordinates:

$$x = X(s,t) + rY'(s,t), \tag{A.1}$$
$$y = Y(s,t) - rX'(s,t), \tag{A.2}$$

where the prime denotes differentiation with respect to the arclength parameter s and $X'(s,t)^2 + Y'(s,t)^2 = 1$.

Natural Basis:

$$\mathbf{g}_1 = \begin{pmatrix} Y'(s) \\ -X'(s) \end{pmatrix}, \quad \mathbf{g}_2 = \begin{pmatrix} X'(s) + rY''(s) \\ Y'(s) - rX''(s) \end{pmatrix}. \tag{A.3}$$

Physical Basis:

$$\hat{\mathbf{r}} \equiv \mathbf{e}_r = \mathbf{g}_1, \quad \hat{\mathbf{s}} \equiv \mathbf{e}_s = \frac{\mathbf{g}_2}{\|\mathbf{g}_2\|} = \frac{1}{\mathfrak{h}}\mathbf{g}_2, \tag{A.4}$$

where $\mathfrak{h} = 1 + r\mathcal{K}$.

Dual Basis:

$$\mathbf{g}^1 = \mathbf{g}_1, \quad \mathbf{g}^2 = \frac{\mathbf{g}_2}{\mathfrak{h}^2}. \tag{A.5}$$

A.1 Gradient of a Scalar

$$\nabla f = \partial_k f \mathbf{g}^k = \partial_r f \hat{\mathbf{r}} + \frac{1}{\mathfrak{h}} \partial_s f \hat{\mathbf{s}} \tag{A.6}$$

A.2 Gradient of a Vector

$$\nabla \mathbf{v} = \left(\partial_k v^i + v^j \Gamma^i_{jk}\right) \mathbf{g}_i \otimes \mathbf{g}^k \tag{A.7}$$

All of the Γ^i_{jk} are zero except for:

$$\Gamma^2_{12} = \Gamma^2_{21} = \frac{\mathcal{K}}{\mathfrak{h}},$$
$$\Gamma^1_{22} = -\mathcal{K}\mathfrak{h},$$
$$\Gamma^2_{22} = \frac{r\mathcal{K}'}{\mathfrak{h}}.$$

Therefore, it follows that the components of $\nabla\mathbf{v}$ in the natural basis are:

$$(\nabla\mathbf{v})^i_k = \begin{pmatrix} \partial_r v^1 & \partial_s v^1 - v^2\mathcal{K}\mathfrak{h} \\ \partial_r v^2 + v^2\dfrac{\mathcal{K}}{\mathfrak{h}} & \partial_s v^2 + v^1\dfrac{\mathcal{K}}{\mathfrak{h}} + v^2\dfrac{r\mathcal{K}'}{\mathfrak{h}} \end{pmatrix} \tag{A.8}$$

In the physical basis, these elements can be readily computed:

$$\begin{pmatrix} \partial_r v^r & \dfrac{1}{\mathfrak{h}}\left(\partial_s v^r - v^s\mathcal{K}\right) \\ \mathfrak{h}\partial_r\left(\dfrac{v^s}{\mathfrak{h}}\right) + v^s\dfrac{\mathcal{K}}{\mathfrak{h}} & \dfrac{1}{\mathfrak{h}}\left(\partial_s v^s + v^r\mathcal{K}\right) \end{pmatrix}. \tag{A.9}$$

Note that the physical components are related to the natural components as follows: $v^r = v^1$, $v^s = hv^2$.

A.3 Divergence of a Second-Order Tensor Field

$$\nabla\cdot\mathrm{S} = \left(\partial_i \mathrm{S}^i_j + \mathrm{S}^l_j\Gamma^i_{il} - \mathrm{S}^i_l\Gamma^l_{ij}\right)\mathbf{g}^j \tag{A.10}$$

$$(\nabla\cdot\mathrm{S})_1 = \partial_1\mathrm{S}^1_1 + \partial_2\mathrm{S}^2_1 + \mathrm{S}^1_1\frac{\mathcal{K}}{\mathfrak{h}} + \mathrm{S}^2_1\frac{r\mathcal{K}'}{\mathfrak{h}} - \mathrm{S}^2_2\frac{\mathcal{K}}{\mathfrak{h}}, \tag{A.11}$$
$$(\nabla\cdot\mathrm{S})_2 = \partial_1\mathrm{S}^1_2 + \partial_2\mathrm{S}^2_2 + \mathfrak{h}\mathrm{S}^2_1\mathcal{K}. \tag{A.12}$$

In terms of the physical components, we have:

$$(\nabla\cdot\mathrm{S})_r = \partial_r\mathrm{S}^r_r + \frac{1}{\mathfrak{h}}\partial_s\mathrm{S}^s_r + \mathrm{S}^r_r\frac{\mathcal{K}}{\mathfrak{h}} - \mathrm{S}^s_s\frac{\mathcal{K}}{\mathfrak{h}}, \tag{A.13}$$
$$(\nabla\cdot\mathrm{S})_s = \mathfrak{h}\partial_r\left(\mathfrak{h}\mathrm{S}^r_s\right) + \mathfrak{h}\partial_s\mathrm{S}^s_s + \mathfrak{h}\mathrm{S}^s_r\mathcal{K}. \tag{A.14}$$

A.4 Tensors from the Theory of Elasticity

From Eq. (A.9) we can compute the strain tensor in these coordinates:

$$\boldsymbol{\epsilon} = \frac{1}{2}\left(\nabla\mathbf{u} + \nabla\mathbf{u}^T\right) = \begin{pmatrix} \partial_r u^r & \dfrac{1}{2}\left(\dfrac{1}{\mathfrak{h}}\partial_s u^r + \mathfrak{h}\partial_r\left(\dfrac{u^s}{\mathfrak{h}}\right)\right) \\ \dfrac{1}{2}\left(\dfrac{1}{\mathfrak{h}}\partial_s u^r + \mathfrak{h}\partial_r\left(\dfrac{u^s}{\mathfrak{h}}\right)\right) & \dfrac{1}{\mathfrak{h}}\left(\partial_s u^s + u^r\mathcal{K}\right) \end{pmatrix}. \tag{A.15}$$

Since the new coordinates are orthogonal and are related with the old ones through a rotation (locally) and the elasticity tensor C_{ijkl} is invariant with respect to rotations, Eq. (2.11d) is still valid. We can write the elements of the stress tensor explicitly:

$$\begin{aligned}\sigma_{rr} &= \frac{2G}{1-2\nu}\left((1-\nu)\epsilon_{rr}+\nu\epsilon_{ss}-(1+\nu)h(c)\right) \qquad \text{(A.16)}\\ &= \frac{2G}{1-2\nu}\left((1-\nu)\partial_r u^r+\frac{\nu}{\mathfrak{h}}\left(\partial_s u^s+u^r\mathcal{K}\right)-(1+\nu)h(c)\right)\end{aligned}$$

$$\sigma_{rs}=\sigma_{sr}=2G\epsilon_{rs}=G\left(\frac{1}{\mathfrak{h}}\partial_s u^r+\mathfrak{h}\partial_r\left(\frac{u^s}{\mathfrak{h}}\right)\right) \qquad \text{(A.17)}$$

$$\begin{aligned}\sigma_{ss} &= \frac{2G}{1-2\nu}\left((1-\nu)\epsilon_{ss}+\nu\epsilon_{rr}-(1+\nu)h(c)\right) \qquad \text{(A.18)}\\ &= \frac{2G}{1-2\nu}\left(\nu\partial_r u^r+\frac{1-\nu}{\mathfrak{h}}\left(\partial_s u^s+u^r\mathcal{K}\right)-(1+\nu)h(c)\right)\end{aligned}$$

In order to write the equations, it is important to obtain the value of the derivative of the elastic energy (Eq. (2.1)). It can be written as follows:

$$\partial_c W(\boldsymbol{\epsilon},c)=\frac{1}{2}\left[-2h'(c)\delta_{ij}\sigma_{ij}+\frac{G'(c)}{G(c)}\left(\epsilon_{ij}-h(c)\delta_{ij}\right)\sigma_{ij}\right] \qquad \text{(A.19)}$$

where the indices run over r, s and z.

We can compute the derivative explicitly in terms of the displacement field:

$$\begin{aligned}\partial_c W(\boldsymbol{\epsilon},c) = {}& (1+\nu)\frac{3(h(c)^2G(c))'}{1-2\nu}\\ &+\frac{(1-\nu)G'(c)}{1-2\nu}\left[(\partial_r u^r)^2+\frac{1}{\mathfrak{h}^2}\left(\partial_s u^s+u^r\mathcal{K}\right)^2\right]\\ &+\frac{1}{\mathfrak{h}}\frac{2\nu G'(c)}{1-2\nu}\partial_r u^r\left(\partial_s u^s+u^r\mathcal{K}\right) \qquad \text{(A.20)}\\ &-\frac{2(1+\nu)(h(c)G(c))'}{1-2\nu}\left[\partial_r u^r+\frac{1}{\mathfrak{h}}\left(\partial_s u^s+u^r\mathcal{K}\right)\right]\\ &+\frac{1}{2}G'(c)\left(\frac{1}{\mathfrak{h}}\partial_s u^r+\mathfrak{h}\partial_r\left(\frac{u^s}{\mathfrak{h}}\right)\right)^2\end{aligned}$$

B Elasticity on the boundary

In this appendix we discuss the continuity of the different elements of the stress and strain tensor. We begin by writing explicitly their form for the order zero, in the inner and in the outer case:

$$\boldsymbol{\epsilon}_0=\begin{pmatrix}\partial_\eta u_{r,1} & \frac{1}{2}\left(\partial_s u_{r,0}+\partial_\eta u_{s,1}-\mathcal{K}u_{s,0}\right)\\ \frac{1}{2}\left(\partial_s u_{r,0}+\partial_\eta u_{s,1}-\mathcal{K}u_{s,0}\right) & \partial_s u_{s,0}+u_{r,0}\mathcal{K}\end{pmatrix} \qquad \text{(B.1)}$$

$$\boldsymbol{\sigma}_0 = \frac{2G(c_0)}{1-2\nu}\begin{pmatrix} (1-\nu)\epsilon_{rr,0} + \nu\epsilon_{ss,0} - (1+\nu)h(c_0) & (1-2\nu)\epsilon_{rs,0} \\ (1-2\nu)\epsilon_{rs,0} & (1-\nu)\epsilon_{ss,0} + \nu\epsilon_{rr_0} - (1+\nu)h(c_0) \end{pmatrix} \tag{B.2}$$

We know from Eqs. (3.11) that the displacement fields (and therefore all their s derivatives) are continuous at the interface.

$$\tilde{\boldsymbol{\epsilon}}_0^{\pm} = \begin{pmatrix} \partial_r \tilde{u}_{r,0}^{\pm} & \frac{1}{2}\left(\partial_s \tilde{u}_{r,0} + \partial_r \tilde{u}_{s,0}^{\pm} - \mathcal{K}\tilde{u}_{s,0}\right) \\ \frac{1}{2}\left(\partial_s \tilde{u}_{r,0} + \partial_r \tilde{u}_{s,0}^{\pm} - \mathcal{K}\tilde{u}_{s,0}\right) & \partial_s \tilde{u}_{s,0} + \tilde{u}_{r,0}\mathcal{K} \end{pmatrix}. \tag{B.3}$$

Hence it follows that $\tilde{\epsilon}_{ss,0}$ is continuous at the interface. Since components rr, rs and sr of the stress tensor are continuous at the interface we obtain two different jump conditions for the strain tensor from the components of the stress tensor at the interface:

$$\tilde{\boldsymbol{\sigma}}_0^{\pm} = \frac{2G(c_0^{\pm})}{1-2\nu}\begin{pmatrix} (1-\nu)\tilde{\epsilon}_{rr,0}^{\pm} + \nu\tilde{\epsilon}_{ss,0} - (1+\nu)h(\tilde{c}_0^{\pm}) & (1-2\nu)\tilde{\epsilon}_{rs,0}^{\pm} \\ (1-2\nu)\tilde{\epsilon}_{rs,0}^{\pm} & (1-\nu)\tilde{\epsilon}_{ss,0} + \nu\tilde{\epsilon}_{rr,0}^{\pm} - (1+\nu)h(\tilde{c}_0^{\pm}) \end{pmatrix} \tag{B.4}$$

From the different jump conditions, we extract the following conditions (no summation):

$$\left(\tilde{\sigma}_{ij,0}^{+} - \tilde{\sigma}_{ij,0}^{-}\right)\left(\tilde{\epsilon}_{ij,0}^{+} - \tilde{\epsilon}_{ij,0}^{-}\right) = 0 \tag{B.5}$$

References

[1] H. Abels and S. Schaubeck. Sharp interface limit for the Cahn-Larche system. *Asymptotic Analysis*, 91(3-4):283–340, 2015.

[2] A. F. Bower, P. R. Guduru, and V. A. Sethuraman. A finite strain model of stress, diffusion, plastic flow, and electrochemical reactions in a lithium-ion half-cell. *Journal of the Mechanics and Physics of Solids*, 59(4):804–828, 2011.

[3] L. Bronsard, H. Garcke, and B. Stoth. A multi-phase Mullins-Sekerka system: matched asymptotic expansions and an implicit time discretisation or the geometric evolution problem. *Proc. Roy. Soc. of Edingburgh: Sec. A Mathematics*, 128:481–06, 1998.

[4] G. Bucci, S. P. Nadimpalli, V. A. Sethuraman, A. F. Bower, and P. R. Guduru. Measurement and modeling of the mechanical and electrochemical response of amorphous Si thin film electrodes during cyclic lithiation. *Journal of the Mechanics and Physics of Solids*, 62:276–294, 2014.

[5] D. Burch and M. Z. Bazant. Size-dependent spinodal and miscibility gaps for intercalation in nanoparticles. *Nano Letters*, 9(11):3795–3800, 2009. PMID: 19824617.

[6] J. Chakraborty, C. P. Please, A. Goriely, and S. J. Chapman. Combining mechanical and chemical effects in the deformation and failure of a cylindrical electrode particle in a li-ion battery. *International Journal of Solids and Structures*, 54:66 – 81, 2015.

[7] J. Chakraborty, C. P. Please, A. Goriely, and S. J. Chapman. Influence of constraints on axial growth reduction of cylindrical li-ion battery electrode particles. *Journal of Power Sources*, 279:746 – 758, 2015. 9th International Conference on Lead-Acid Batteries {LABAT} 2014.

[8] E. D. Cubuk and E. Kaxiras. Theory of structural transformation in lithiated amorphous silicon. *Nano Lett.*, 14(7):4065–4070, Jul 2014.

[9] Z. Cui, F. Gao, and J. Qu. A finite deformation stress-dependent chemical potential and its applications to lithium ion batteries. *Journal of the Mechanics and Physics of Solids*, 60(7):1280–1295, 2012.

[10] P. Fratzl, O. Penrose, and J. L. Lebowitz. Modeling of phase separation in alloys with coherent elastic misfit. *Journal of Statistical Physics*, 95(5-6):1429–1503, June 1999.

[11] E. Fried and M. E. Gurtin. Dynamic solid-solid transitions with phase characterized by an order parameter. *Physica D: Nonlinear Phenomena*, 72(4):287–308, 1994.

[12] H. Garcke. On Cahn-Hilliard systems with elasticity. *Proceedings of the Royal Society of Edinburgh: Section A Mathematics*, 133(02):307–331, 2003.

[13] H. Garcke and D. J. C. Kwak. On asymptotic limits of Cahn-Hilliard systems with elastic misfit. In A. Mielke, editor, *Analysis, modeling and simulation of multiscale problems*, pages 87–111. Springer, 2006.

[14] Y. Huang, D. Ngo, and A. Rosakis. Non-uniform, axisymmetric misfit strain: in thin films bonded on plate substrates/substrate systems: the relation between non-uniform film stresses and system curvatures. *Acta Mechanica Sinica*, 21(4):362–370, 2005.

[15] P. Leo, J. Lowengrub, and H.-J. Jou. A diffuse interface model for microstructural evolution in elastically stressed solids. *Acta materialia*, 46(6):2113–2130, 1998.

[16] P. Leo and R. Sekerka. Overview no. 86: The effect of surface stress on crystal-melt and crystal-crystal equilibrium. *Acta Metallurgica*, 37(12):3119 – 3138, 1989.

[17] P. H. Leo and R. Sekerka. The effect of elastic fields on the morphological stability of a precipitate grown from solid solution. *Acta metallurgica*, 37(12):3139–3149, 1989.

[18] V. I. Levitas and H. Attariani. Anisotropic compositional expansion in elastoplastic materials and corresponding chemical potential: Large-strain formulation and application to amorphous lithiated silicon. *Journal of the Mechanics and Physics of Solids*, 69:84–111, Sep 2014.

[19] X. H. Liu, F. Fan, H. Yang, S. Zhang, J. Y. Huang, and T. Zhu. Self-limiting lithiation in silicon nanowires. *ACS Nano*, 7(2):1495–1503, Feb 2013.

[20] M. T. McDowell, S. W. Lee, J. T. Harris, B. A. Korgel, C. Wang, W. D. Nix, and Y. Cui. In situ tem of two-phase lithiation of amorphous silicon nanospheres. *Nano letters*, 13(2):758–764, 2013.

[21] M. T. McDowell, S. W. Lee, W. D. Nix, and Y. Cui. 25th anniversary article: Understanding the lithiation of silicon and other alloying anodes for lithium-ion batteries. *Advanced Materials*, 25(36):4966–4985, 2013.

[22] E. Meca, A. Münch, and B. Wagner. Thin-film electrodes for high-capacity lithium-ion batteries: Influence of phase transformations on stress. Preprint-5-2016, Institute of Mathematics, Technical University Berlin, 2016.

[23] E. Meca, V. B. Shenoy, and J. Lowengrub. Phase-field modeling of two-dimensional crystal growth with anisotropic diffusion. *Phys. Rev. E*, 88:052409, Nov 2013.

[24] D. Ngo, Y. Huang, A. Rosakis, and X. Feng. Spatially non-uniform, isotropic misfit strain in thin films bonded on plate substrates: The relation between non-uniform film stresses and system curvatures. *Thin Solid Films*, 515(4):2220–2229, 2006.

[25] A. Novick-Cohen. On the viscous Cahn-Hilliard equation. Material instabilities in continuum mechanics, Edinburgh, 1985–1986, 329–342. *Oxford Sci. Publ., Oxford Univ. Press, New York*, 1988.

[26] N. Owen, J. Rubinstein, and P. Sternberg. Minimizers and gradient flows for singularly perturbed bi-stable potentials with a Dirichlet dondition. *Proc. R. Soc. Lond. A*, 429:505–532, 1990.

[27] R. L. Pego. Front migration in the nonlinear Cahn-Hilliard equation. *Proceedings of the Royal Society of London A: Mathematical, Physical and Engineering Sciences*, 422(1863):261–278, 1989.

[28] V. A. Sethuraman, M. J. Chon, M. Shimshak, V. Srinivasan, and P. R. Guduru. In situ measurements of stress evolution in silicon thin films during electrochemical lithiation and delithiation. *Journal of Power Sources*, 195(15):5062–5066, 2010.

[29] V. Shenoy, P. Johari, and Y. Qi. Elastic softening of amorphous and crystalline Li–Si phases with increasing Li concentration: a first-principles study. *Journal of Power Sources*, 195(19):6825–6830, 2010.

[30] J. W. Wang, Y. He, F. Fan, X. H. Liu, S. Xia, Y. Liu, C. T. Harris, H. Li, J. Y. Huang, S. X. Mao, and et al. Two-phase electrochemical lithiation in amorphous silicon. *Nano Lett.*, 13(2):709–715, Feb 2013.

[31] S. Wise, J. Kim, and J. Lowengrub. Solving the regularized, strongly anisotropic Cahn-Hilliard equation by an adaptive nonlinear multigrid method. *Journal of Computational Physics*, 226(1):414 – 446, 2007.

[32] Y. Zeng and M. Z. Bazant. Phase separation dynamics in isotropic ion-intercalation particles. *SIAM Journal on Applied Mathematics*, 74(4):980–1004, 2014.

[33] K. Zhao, G. A. Tritsaris, M. Pharr, W. L. Wang, O. Okeke, Z. Suo, J. J. Vlassak, and E. Kaxiras. Reactive flow in silicon electrodes assisted by the insertion of lithium. *Nano Lett.*, 12(8):4397–4403, Aug 2012.